









RESEARCH ARTICLE | FEBRUARY 22 2024

Vibrational state-specific nonadiabatic photodissociation dynamics of OCS^+ via $A^2\Pi_{1/2} (v_1 0 v_3)$ states

Yaling Wang ; Yunfan Zhao; Ning Zhang; Wenxin Wang; Liru Hu; Chang Luo ; Daofu Yuan  ; Xiaoguo Zhou ; David H. Parker ; Xueming Yang ; Xingan Wang  



J. Chem. Phys. 160, 084301 (2024)

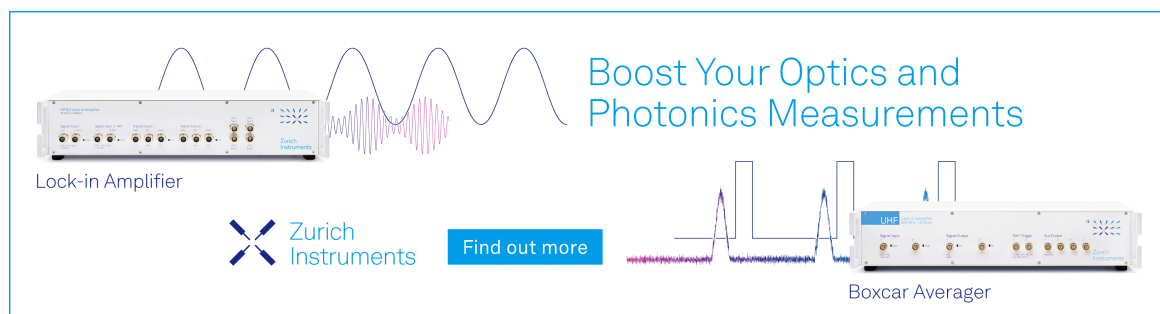
<https://doi.org/10.1063/5.0191893>



View
Online




Export
Citation



Boost Your Optics and
Photonics Measurements

Lock-in Amplifier

 Zurich
Instruments

[Find out more](#)

Boxcar Averager

Vibrational state-specific nonadiabatic photodissociation dynamics of OCS^+ via $A^2\Pi_{1/2} (\nu_1 0 \nu_3)$ states

Cite as: J. Chem. Phys. 160, 084301 (2024); doi: 10.1063/5.0191893

Submitted: 17 December 2023 • Accepted: 29 January 2024 •

Published Online: 22 February 2024



View Online



Export Citation



CrossMark

Yaling Wang,¹ Yunfan Zhao,¹ Ning Zhang,¹ Wenxin Wang,¹ Liru Hu,¹ Chang Luo,¹ Daofu Yuan,^{1,a)} Xiaoguo Zhou,¹ David H. Parker,² Xueming Yang,^{3,4,5} and Xingan Wang^{1,5,a)}

AFFILIATIONS

¹Hefei National Research Center for Physical Science at the Microscale and Department of Chemical Physics, University of Science and Technology of China, Hefei 230026, China

²Department of Molecular and Laser Physics, Institute for Molecules and Materials, Radboud University, Heyendaalseweg 135, 6525 AJ Nijmegen, The Netherlands

³State Key Laboratory of Molecular Reaction Dynamics, Dalian Institute of Chemical Physics, Chinese Academy of Sciences, Dalian 116023, China

⁴Department of Chemistry, School of Science, Southern University of Science and Technology, Shenzhen 518055, China

⁵Hefei National Laboratory, Hefei 230088, China

^{a)}Authors to whom correspondence should be addressed: ydfu@ustc.edu.cn and xawang@ustc.edu.cn

ABSTRACT

The identification and analysis of quantum state-specific effects can significantly deepen our understanding of detailed photodissociation dynamics. Here, we report an experimental investigation on the vibrational state-mediated photodissociation of the OCS^+ cation via the $A^2\Pi_{1/2} (\nu_1 0 \nu_3)$ states by using the velocity map ion imaging technique over the photolysis wavelength range of 263–294 nm. It was found that the electronically excited S^+ product channel $S^+ (^2D_u) + \text{CO} (X^1\Sigma^+)$ was significantly enhanced when the ν_1 and ν_3 vibrational modes were excited. Clear deviations in the branching ratios of the electronically excited S^+ channel were observed when the vibrational modes ν_1 and ν_3 were selectively excited. The results reveal that vibrationally excited states play a vital role in influencing the nonadiabatic couplings in the photodissociation process.

Published under an exclusive license by AIP Publishing. <https://doi.org/10.1063/5.0191893>

INTRODUCTION

Quantum state-specific effects are important in the study of chemical reaction dynamics.^{1–4} Over the past decades, their influence over unimolecular and bimolecular reaction dynamics has successfully been investigated through the manipulation of internal motions,⁵ primarily via vibrational state excitation, offering a potential avenue for efficiently affecting reaction pathways. The vibrational-state-mediated process has been studied in the photodissociation of neutral molecules, such as HNO_3 ,^{6,7} H_2O_2 ,^{8,9} H_2O ,^{2,10} and BuOOH .¹¹ In particular, it is worth noting that in the work of Vander Wal and Crim,² four-quanta excitation in the O–H stretching vibration of HOD resulted in the selective cleavage of

the O–H bond. Nevertheless, the excitation of multiple vibrational modes simultaneously within a molecule with a single photon is experimentally difficult. Regarding molecular ions, precise preparation of specific vibrationally excited states remains challenging. The current understanding of mode-selective and state-selective photodissociation dynamics is still lacking, especially for molecular ions.

Carbonyl sulfide (OCS) is the predominant sulfur-containing compound in the Earth's atmosphere.^{12,13} A high-resolution photoelectron spectrum of OCS shows three well-defined excited electronic states of OCS^+ , namely, $A^2\Pi$, $B^2\Sigma^+$, and $C^2\Sigma^+$, which bear a resemblance to those of CO_2^+ .¹⁴ In a study carried out by Eland in 1973,¹⁵ it was predicted that the photodissociation process of OCS^+

could be significantly influenced by vibronic coupling. In 2005, Chang *et al.* conducted an experimental study on the mode-selected predissociation of OCS^+ via the $\text{B}^2\Sigma^+(v_1 v_2 v_3)$ excited states using the velocity map ion imaging (VMI) technique.¹⁶ Compared to the $\text{B}^2\Sigma^+$ state, there exists a substantial amount of research focused on $\text{OCS}^+(\text{A}^2\Pi)$,^{15,20,31,34} which offers the possibility of a detailed understanding of state-mediated dynamics. The $\text{OCS}^+(\text{A}^2\Pi_{1/2})$ cation exhibits three distinct vibrational modes, and their approximate types of modes are C–S stretch (v_1), bending (v_2), and C–O stretch (v_3), respectively. The fundamental vibrational frequencies of these three modes were determined to be around 802, 354, and 2028 cm^{-1} , respectively.^{14,17–20} The well-defined low-lying electronic states and vibrational structures of OCS^+ make it a suitable candidate for the investigation of vibrational state-specific photochemistry processes. Here, we report an experimental study on the quantum state-specific effect in the photodissociation of the OCS^+ cation. The measurements were performed by using a double resonance strategy, which allowed for a high-resolution investigation of a quantum state-specific photodissociation process. During this procedure, the neutral molecule was first laser-ionized using resonance-enhanced multi-photon ionization (REMPI). After a short delay, the prepared cations were excited to a specific excited vibronic state, resulting in the production of fragments. Various successful investigations^{16,21–30} on molecular cations have been conducted utilizing this method.

Over the past decades, experimental and theoretical studies have been focusing on two nonadiabatic photodissociation channels via the $\text{A}^2\Pi$ state, which are the $\text{S}^+(^4\text{S}_u) + \text{CO}(\text{X}^1\Sigma^+)$ and $\text{S}^+(^2\text{D}_u) + \text{CO}(\text{X}^1\Sigma^+)$ channels. Chen *et al.*³¹ calculated the dissociation energies (D_e) of the product channels, $\text{S}^+(^4\text{S}) + \text{CO}$ and $\text{S}^+(^2\text{D}) + \text{CO}$, at the CASPT2/ANO-L//CASSCF/ANO-S (2.01 and 3.92 eV) and CASPT2/ANO-S//CASSCF/ANO-S (1.52 and 3.71 eV) levels of theory. The dissociation limits were experimentally measured to be 2.31 eV [$\text{S}^+(^4\text{S}) + \text{CO}$ channel] and 4.15 eV [$\text{S}^+(^2\text{D}) + \text{CO}$ channel] using photoelectron–photoion coincidence spectroscopy.¹⁵ As proposed, the $\text{S}^+(^4\text{S}_u) + \text{CO}(\text{X}^1\Sigma^+)$ dissociation channel correlated with the $1^4\Sigma^-$ repulsive state.¹⁵ The predissociation via the $\text{A}^2\Pi$ state could take place in two ways: either through direct coupling from the $\text{A}^2\Pi$ state to the $1^4\Sigma^-$ state or through internal conversion (IC) to the ground electronic state ($\text{X}^1\Sigma^+$) of the molecular ions, followed by coupling to the $1^4\Sigma^-$ state. Wu *et al.*³² suggested that a curve crossing between the $\text{A}^2\Pi$ and $1^4\Sigma^-$ surfaces was involved in the dissociation of OCS^+ , leading to the $\text{S}^+(^4\text{S}_u) + \text{CO}(\text{X}^1\Sigma^+)$ channel. However, Hubin-Franskin *et al.*³³ proposed that the $\text{A}^2\Pi$ state should undergo decay to the $\text{X}^2\Pi$ state, which is subsequently followed by predissociation to the lowest limit. Hirst³⁴ also suggested that the primary dissociation mechanism is unlikely to be spin–orbit coupling between the $\text{A}^2\Pi$ and $1^4\Sigma^-$ states. As for the second dissociation channel $\text{S}^+(^2\text{D}_u) + \text{CO}(\text{X}^1\Sigma^+)$ via the $\text{A}^2\Pi$ state, previous studies have also presented two potential routes. In 1969, Judge and Ogawa³⁵ examined the likelihood of the predissociation of OCS^+ via the $\text{A}^2\Pi$ state into the second limit being correlated with the $^2\Sigma^-$ and $^2\Delta$ states. Chen *et al.*³¹ calculated the relative energies corresponding to the minimum positions along the intersection seams of $\text{A}^2\Pi$ – $^2\Sigma^-$ and $\text{A}^2\Pi$ – $^2\Delta$. Hubin-Franskin *et al.*³³ proposed an alternative pathway involving IC from the $\text{A}^2\Pi$ state to the $\text{X}^2\Pi$ state, followed by adiabatic unimolecular decomposition, as inferred from their utilization of threshold photoelectron–photoion coincidence

spectroscopy in conjunction with *ab initio* calculations. Hirst³⁴ has suggested that the significance of spin–orbit coupling between the $\text{A}^2\Pi$ and $^2\Sigma^-/^2\Delta$ states is minor due to the fact the dominant configuration for the $\text{A}^2\Pi$ state within the potential well exhibits a deviation of more than two spin-orbital points from the dissociative states.

Previous studies¹⁵ have revealed that vibronic coupling plays a significant role, and that vibrational excitation in the final state is a crucial determinant in controlling the predissociation rate of OCS^+ in the $\text{A}^2\Pi$ state. To obtain more detailed dynamic information about the state-specific photodissociation behavior, high-resolution experimental studies on the photodissociation of OCS^+ via well-defined $\text{A}^2\Pi(v_1 v_2 v_3)$ excited states are essential. The time-sliced VMI technique is a widely utilized detection method that enables high-resolution detection of the speed and angular distribution of products. The time-sliced VMI ion optics, originally designed by Lin *et al.*,³⁶ served as the foundational framework for our ion imaging system and has been employed in the investigation of the photodissociation dynamics of a variety of neutral molecules, including the N_2O and OCS molecules.^{37–43}

In this study, we investigate OCS^+ photodissociation using VMI techniques via five well-prepared vibrational levels of the $\text{A}^2\Pi_{u,1/2}(v_1 v_2 v_3)$ states in the UV region. High-resolution images of the S^+ fragments were acquired. The kinetic energy distributions, branching ratios, and angular distributions of the $\text{S}^+(^4\text{S}_u) + \text{CO}(\text{X}^1\Sigma^+)$ and $\text{S}^+(^2\text{D}_u) + \text{CO}(\text{X}^1\Sigma^+)$ dissociation channels were determined. The results revealed that the branching ratios of $\text{S}^+(^4\text{S}_u)$ and $\text{S}^+(^2\text{D}_u)$ products presented significant vibrational state-specific behavior, which was shown to be sensitive to the excitation of vibrational states of OCS^+ in the $\text{A}^2\Pi$ state. A notable deviation in the branching ratios of the $\text{S}^+(^2\text{D}_u) + \text{CO}(\text{X}^1\Sigma^+)$ channel was observed when the vibrational modes v_1 and v_3 were selectively excited. The results reveal that vibrational excitation plays a key role in the dissociation process.

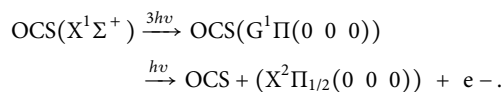
EXPERIMENTAL METHOD

The photodissociation experiments were carried out using a time-sliced VMI apparatus, and the details of the experiment have been described previously.⁴⁴ The apparatus consists of one source chamber and one detection chamber. These two differentially pumped vacuum chambers were evacuated by using turbomolecular pumps with pumping speeds of 1600 and 700 l/s, respectively. The typical operating pressures in the source chamber and the detection chamber were 1×10^{-5} – 2×10^{-5} and 1×10^{-7} – 5×10^{-7} mbar, respectively.

A gas mixture containing 10% OCS in Ar was supersonically expanded by a pulsed valve (general valve, Parker Series 9) with a 1 mm orifice to form the OCS molecular beam. The pulsed valve operated at a repetition rate of 20 Hz, and the stagnation pressure behind the nozzle was 1 bar. The OCS molecule beam was skimmed and collimated by a conical skimmer with a 1.5 mm orifice before intersecting the photoionization laser inside the ion optics.

After passing through a 2 mm hole on the first repeller plate of the ion optics, OCS underwent two processes of ionization and photodissociation in the reaction center that is located between the second and third plates of the ion optics. By fixing the ionization

laser at 419.86 nm, the (3 + 1) resonance-enhanced multi-photon ionization (REMPI) scheme could be achieved,



The ionization laser with a power of about 3.0 mJ/pulse was provided by a pulsed dye laser (Sirah, Cobra Stretch) pumped by an Nd:YAG laser (Continuum, Powerlite 9020), which was focused perpendicularly on the molecular beam of OCS by a quartz lens with $f = 200$ mm. The repetition rate of the laser system is 20 Hz. To eliminate the possible influence of ionization laser polarization on the spatial distribution of photoproducts, the ionization laser used in our experiment is circularly polarized.

After a short delay, the OCS^+ beam was photodissociated by another counter-propagated laser whose wavelength was scanned in the range of 263–294 nm. We obtained a series of resonance peaks shown in the photofragment excitation spectrum (PHOFEX). Based on the known vibrational frequencies, all spectral features can be assigned to the $A^2\Pi_{1/2}(v_1\ v_2\ v_3) \leftarrow X^2\Pi(0\ 0\ 0)$ vibronic transition of the OCS^+ cations, which were consistent with the PHOFEX spectra reported by Weinkauff and Boesl.¹⁹

The photolysis laser with a power of 1 mJ/pulse was produced by doubling the output of a second dye laser (Sirah, Cobra Stretch), which was pumped by another Nd:YAG laser (Beamtech, SGR-20). The photolysis laser was focused by a fused quartz lens with $f = 300$ mm. The polarization of photodissociation is parallel to the plate of the detector. Two dye lasers overlap spatially in the reaction region but with a temporal separation of about 40 ns to ensure the ionization prior to photodissociation in the time scale.

The OCS^+ cations were dissociated into the $\text{S}^+ + \text{CO}$ fragment pair when the wavelengths of the photolysis laser were fixed at each of the five resonance peaks in the PHOFEX spectra. Finally, under the rejection of the electric field, the product ions S^+ were accelerated to reach a dual microchannel plate (MCP) detector with a 75 mm diameter. The two MCP plates were held at 800 and 1200 V, respectively. When the electron arrived at the MCP, a fast high-voltage pulse (400 V, 30 ns duration) was applied to the second MCP plate to gate the MCP for mass selection and time slicing of the ion packet. Multiplier electrons are produced to strike the phosphor screen (P43) that is coupled with MCPs. The P43 phosphor was held at 4500 V higher than the second MCP plate. As a result, the images produced from the P43 phosphor were recorded by a CCD device (LaVision, Imager pro plus 2M), followed by event counting data analysis. All the timings in this work were controlled by two digital delay generators (Stanford Research System, DG 645).

RESULT AND DISCUSSION

Figure 1 shows the VMI images of the S^+ products taken at five wavelengths: 294.26, 287.44, 280.91, 277.95, and 263.57 nm, respectively, based on the PHOFEX spectra of OCS^+ and the corresponding assignment of the $A^2\Pi_{1/2}(v_1\ v_2\ v_3) \leftarrow X^2\Pi(0\ 0\ 0)$ transition reported by Weinkauff and Boesl.¹⁹ These wavelengths correspond to the resonant excitations of the ground vibrational state of OCS^+ in the $X^2\Pi$ state to different vibrational levels of $A^2\Pi_{u,1/2}(v_1\ v_2\ v_3)$: (1 0 1), (2 0 1), (3 0 1), (1 0 2), and (1 0 3),

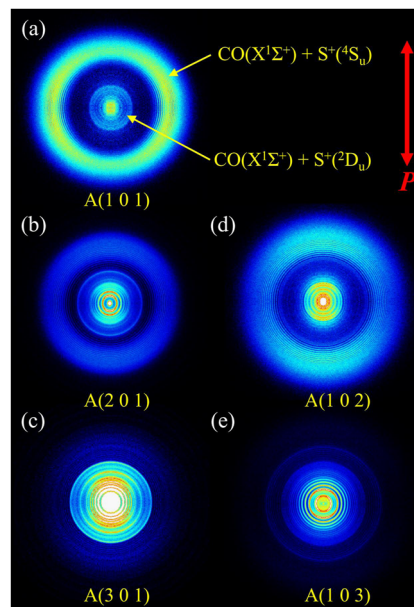


FIG. 1. Experimental images of the $\text{S}^+(^4\text{S}_u)/\text{S}^+(^2\text{D}_u)$ products resulting from the photodissociation of OCS^+ via (a) the $A^2\Pi_{u,1/2}(1\ 0\ 1)$ level at 294.26 nm, (b) the $A^2\Pi_{u,1/2}(2\ 0\ 1)$ level at 287.44 nm, (c) the $A^2\Pi_{u,1/2}(3\ 0\ 1)$ level at 280.91 nm, (d) the $A^2\Pi_{u,1/2}(1\ 0\ 2)$ level at 277.95 nm, and (e) the $A^2\Pi_{u,1/2}(1\ 0\ 3)$ level at 263.57 nm, respectively. The double arrow indicates the polarization direction of the dissociation laser. The rings in the images correspond to the rovibrational state of the coincident CO products.

respectively. In the following text, the electronic state $A^2\Pi_{u,1/2}(v_1\ v_2\ v_3)$ will be abbreviated as $A(v_1\ v_2\ v_3)$. The red vertical arrow indicates the polarization direction of the photolysis laser. The presented images exhibit well-resolved rings with varying brightness, which directly correspond to the two-dimensional recoil velocities of the S^+ products in the center-of-mass (CM) velocity frame. At all photolysis wavelengths, two dissociation channels, specifically, $\text{S}^+(^4\text{S}_u) + \text{CO}(X^1\Sigma^+)$ and $\text{S}^+(^2\text{D}_u) + \text{CO}(X^1\Sigma^+)$ were clearly identified as two bands in the images, as shown in Fig. 1. As denoted by the yellow arrows, the inner rings with lower kinetic energies correspond to the $\text{S}^+(^2\text{D}_u) + \text{CO}(X^1\Sigma^+)$ channel, while the outer rings are associated with the $\text{S}^+(^4\text{S}_u) + \text{CO}(X^1\Sigma^+)$ channel. Moreover, the resolved rings observed on each band correspond to the rovibrational structures of the coincidental CO fragments.

In the case of the $A(1\ 0\ 1)$ excited state, the image exhibited distinct dim inner rings and bright outer rings, indicating that the predominant products formed are $\text{S}^+(^4\text{S}_u)$. A higher abundance of the $\text{S}^+(^2\text{D}_u)$ products was detected in the images of the $A(1\ 0\ 3)$ and $A(3\ 0\ 1)$ excited states compared to the $\text{S}^+(^4\text{S}_u)$ products. For other excited states, direct identification of the ratios between the $\text{S}^+(^4\text{S}_u)$ and $\text{S}^+(^2\text{D}_u)$ channels from the images is not feasible. Further quantitative information regarding this topic will be explored in the subsequent sections (*vide infra*). Regarding the angular distribution of the fragments, with the exception of $A(1\ 0\ 1)$, the products $\text{S}^+(^4\text{S}_u)$ for all other $A(v_1\ v_2\ v_3)$ excited states are mainly distributed along the polarization direction of the photolysis laser. Each ring of the $\text{S}^+(^2\text{D}_u)$ products displayed a distinct spatial distribution with

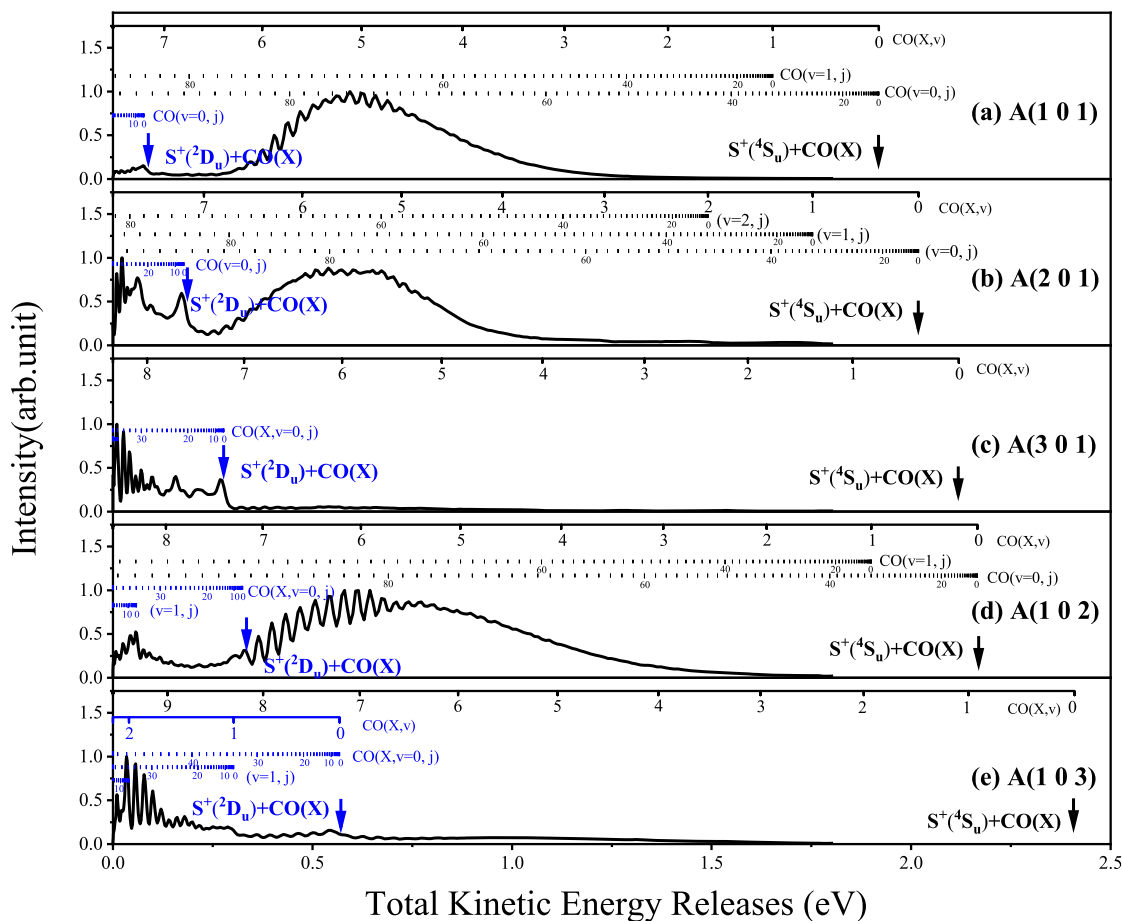


FIG. 2. Total kinetic energy release (TKER) distribution for the $\text{CO}(X^1\Sigma^+) + \text{S}^+(^4\text{S}_u)$ and $\text{CO}(X^1\Sigma^+) + \text{S}^+(^2\text{D}_u)$ channels from the photodissociation of OCS^+ via (a) the $\text{A}^2\Pi_{u,1/2}(1 0 1)$ level, (b) the $\text{A}^2\Pi_{u,1/2}(2 0 1)$ level, (c) the $\text{A}^2\Pi_{u,1/2}(3 0 1)$ level, (d) the $\text{A}^2\Pi_{u,1/2}(1 0 2)$ level, and (e) the $\text{A}^2\Pi_{u,1/2}(1 0 3)$ level, respectively. Assignment combs marked on the top of each panel correspond to the rovibrational energy levels of the co-fragment CO.

anisotropic features in characters. Both the velocity distribution and the spatial distribution of $\text{S}^+(^4\text{S}_u)/\text{S}^+(^2\text{D}_u)$ displayed a vibrational state dependence.

The total kinetic energy release (TKER) spectra of the photodissociation processes derived from the images are shown in Fig. 2. The TKER of the S^+ and CO products can be characterized using Eq. (1). Additionally, the TKER spectra display the partially resolved rotational features of CO, and the rovibrational distribution of CO ($X^1\Sigma^+$) co-fragments can be assigned based on the law of energy conservation,

$$\text{TKER} = E_{\text{hv}} - D_0(\text{S}^+ - \text{CO}) - E_{\text{vib}}(\text{CO}) - E_{\text{rot}}(\text{CO}) - E_{\text{int}}(\text{S}^+), \quad (1)$$

where E_{hv} is the photon energy of the photolysis laser and $D_0(\text{S}^+ - \text{CO})$ is the bond energy of S–C in parent OCS^+ cations on the ground state. In addition, $D_0(\text{S}^+ - \text{CO})$ was determined to be 2.296 eV based on the onset position of the $\text{S}^+(^2\text{D}) + \text{CO}(X^1\Sigma^+)$ channel denoted by the blue arrows shown in Fig. 2, in combination with the energy separation (1.8415 eV) between the $\text{S}^+(^2\text{D})$ and

$\text{S}^+(^4\text{S})$ states; $E_{\text{vib}}(\text{CO})$ and $E_{\text{rot}}(\text{CO})$ are the vibrational and rotational energies of $\text{CO}(X^1\Sigma^+)$ fragments; and $E_{\text{int}}(\text{S}^+)$ is the energy difference between the S^+ products and the ground state $\text{S}^+(^4\text{S}_u)$.

Based on the TKER spectra shown in Fig. 2, it appears that a significant portion of the available energy is carried away by internal excitation of the fragments CO and S^+ . For the A(1 0 1), A(2 0 1), A(3 0 1), A(1 0 2), and A(1 0 3) predissociation states, 69%, 81%, 93%, 73%, and 90% of the available energy were deposited into the internal energy of products, respectively. The experimental results indicate that the CO products from the $\text{S}^+(^4\text{S}_u) + \text{CO}(X^1\Sigma^+)$ channel exhibit a high degree of rotational excitation. Additionally, it was observed that the vibrational state distributions of $\text{CO}(X^1\Sigma^+)$ are modified by the C–S stretching vibrational mode (ν_1) of $\text{OCS}^+(\text{A}^2\Pi)$. As an example, the internal energy distribution of CO(X) via the A(1 0 1) predissociative state is predominantly distributed at $v = 0, 1$. However, via A(2 0 1), the resulting CO(X) products can mainly be assigned to $v = 0, 1, 2$. The rotational assignments of the CO(X) products come from the observable spacings between successive maxima in the TKER spectra and are a reference to the superposed

TABLE I. The average β values of S^+ ions for two product channels via five different vibrationally mediated states.

Assignment	The average β value of S^+	
	$S^+(^4S_u) + CO(X^1\Sigma^+)$	$S^+(^2D_u) + CO(X^1\Sigma^+)$
$A^2\Pi_{u,1/2}(1\ 0\ 1)$	-0.16	0.42
$A^2\Pi_{u,1/2}(2\ 0\ 1)$	0.55	0.57
$A^2\Pi_{u,1/2}(3\ 0\ 1)$	0.52	0.50
$A^2\Pi_{u,1/2}(1\ 0\ 2)$	0.65	0.53
$A^2\Pi_{u,1/2}(1\ 0\ 3)$	0.65	0.42

combs. A similar phenomenon has been observed by Chang *et al.*¹⁶ and Hubin-Franskin *et al.*³³ Hubin-Franskin *et al.* have provided a qualitative interpretation suggesting that the outer crossing point associated with the C–S motion tends to approach the crossing point more closely as the level of CO vibrational excitation is increased. However, the interpretation of the branching ratio for the $v = 1/v = 2$ products remains challenging, primarily because of the substantial overlap observed in the rovibrational features. As for the $S^+(^2D_u) + CO(X^1\Sigma^+)$ channel, it is straightforward to assign the internal energy distribution of $CO(X^1\Sigma^+, v, j)$. The $CO(X^1\Sigma^+)$ products also exhibited a high level of rotational excitation.

The anisotropy parameter (β value) of an angular distribution was determined by fitting the data with Eq. (2). The intensity was integrated over the radial range for each channel from the experimental images,

$$I(\theta) = (1/4\pi)(1 + \beta P_2(\cos \theta)), \quad (2)$$

where P_2 is the second-order Legendre polynomial and θ is the angle between the polarization vector of the photolysis laser and the recoil velocity vector of the S^+ products. The β value ranges from -1 to 2 , providing insights into both the photodissociation dynamics and the symmetry of the excited states. The average β values for two product channels at five wavelengths are presented in Table I. The results show that the β values range from -0.16 to 0.65 , and with the exception of the $S^+(^4S_u)$ channel from the $A(1\ 0\ 1)$ predissociation state, the β values are all around 0.5 , exhibiting the characteristics of parallel photodissociation. The negative β value observed for the $S^+(^4S_u)$ product via the $A(1\ 0\ 1)$ state suggests that the out-plane component of the transition dipole may be responsible for the perpendicular transition. An in-depth justification of the negative β value requires intricate calculations that are beyond the scope of this particular study.

In contrast to laser state-specific resonant ionization for detecting neutral products, the detection of S^+ ions with the VMI method allows for simultaneous coverage of all quantum states of the S^+ ion and the CO co-product. This comprehensive approach provides a robust way for accurately determining the branching ratios for different dissociation channels. The plot in Fig. 3 illustrates the dependence of the branching ratios of the $S^+(^2D_u) + CO(X^1\Sigma^+)$ product channel on the vibrational excitation energy of $A^2\Pi_{u,1/2}(v_1\ v_2\ v_3)$ relative to $A^2\Pi_{u,1/2}(0\ 0\ 0)$ acquired by integrating the TKER spectra shown in Fig. 2. The total fraction of the two channels is normalized, and only the fraction pertaining to the

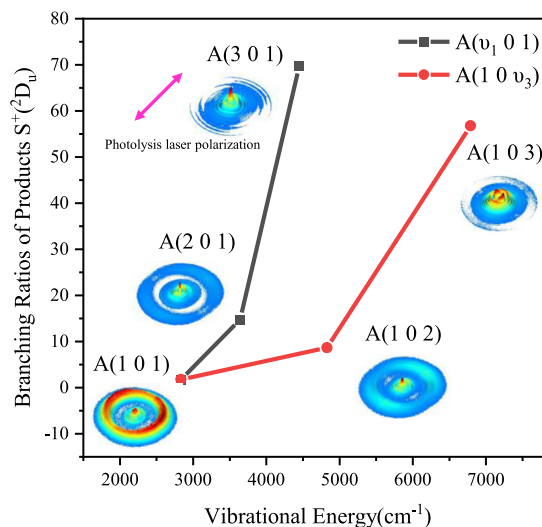


FIG. 3. The 2D plots show branching ratios of the $S^+(^2D_u)$ product for the $S^+(^2D_u) + CO(X^1\Sigma^+)$ dissociation channel via five different vibrational intermediate states of OCS^+ . The experimental images via five different vibrational intermediate states of OCS^+ are also included; the concentric rings represent different S product channels. The double arrow denotes the polarization direction of the photolysis laser.

$S^+(^2D_u) + CO(X^1\Sigma^+)$ channel is shown in Fig. 3. Basically, as the energy of the photon exceeds the threshold of the second dissociation channel, an increasing fraction of the resultant products is usually observed as the excitation energy increases. This regular pattern is consistent with the tendency shown in Fig. 3 that the fraction of the $S^+(^2D_u) + CO(X^1\Sigma^+)$ channel increases in a similar way for $A(v_1\ 0\ 1)$ and $A(1\ 0\ v_3)$ predissociation states with an increase in the vibrational energy or excitation energy.

Interestingly, differences in the branching ratio behaviors are also noticed between the excitation of the two different modes. The excitation of the v_1 vibrational mode of the $A^2\Pi_{u,1/2}$ state leads to a more pronounced enhancement in the formation of the electronically excited product channel $CO(X^1\Sigma^+) + S^+(^2D_u)$ compared to the excitation of the v_3 mode. The manifestation of this intermediate state-dependent photodissociation behavior can be elucidated through two specific aspects: the vibrational quantum number and the total vibrational energy of the excited state. In terms of the vibrational quantum number, the $S^+(^2D_u) + CO(X^1\Sigma^+)$ channel exhibits branching ratios of 9% and 57% for the $A(1\ 0\ 2)$ and $A(1\ 0\ 3)$ excited states, respectively. In comparison, the values are 15% and 70% for the excitation of two [$A(2\ 0\ 1)$ state] and three [$A(3\ 0\ 1)$ state] quanta of the v_1 mode, respectively. From the perspective of the total vibrational energy, it is noteworthy that the $A(3\ 0\ 1)$ predissociation state has a lower total vibrational energy (4449 cm^{-1}) compared to the $A(1\ 0\ 2)$ state (4827 cm^{-1}). However, the proportion of the excited dissociation channel $S^+(^2D_u) + CO(X^1\Sigma^+)$ resulting from the $A(3\ 0\ 1)$ intermediate state is more than sevenfold larger than that for the $A(1\ 0\ 2)$ state. The present study observed a vibrational state-specific photodissociation behavior wherein the promotion of the formation of the electronically excited $S^+(^2D_u) + CO(X^1\Sigma^+)$ channel, which has a higher dissociation threshold, is more pronounced

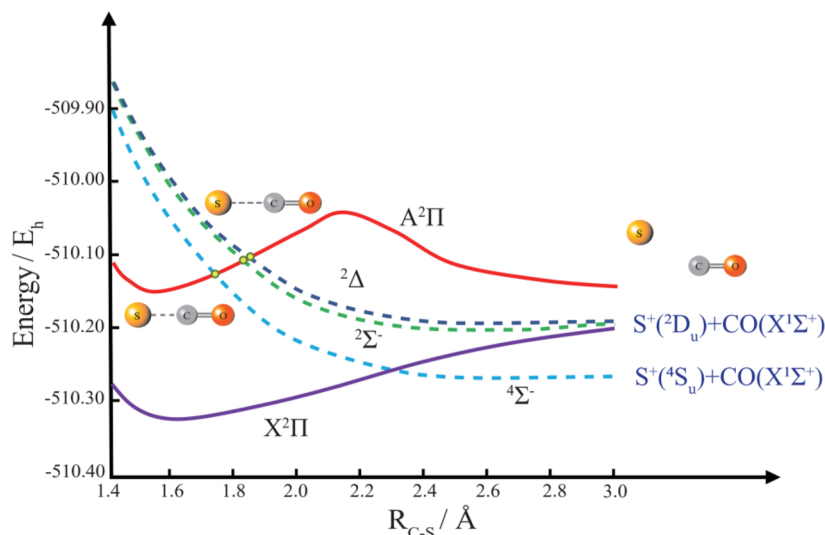


FIG. 4. Schematic of potential-energy curves along the C–S coordinate (adapted from Ref. 34). The red solid line and the purple solid line represent the ground electronic state $X^2\Pi$ and the first excited electronic state $A^2\Pi$, respectively. The blue dotted line, the green dotted line, and the dark blue dotted line represent the repulsive states $1^4\Sigma^-$, $2^2\Sigma^-$, and $2^2\Delta$, respectively.

when the vibrational mode with a lower frequency is excited, as opposed to when the vibrational mode with a higher frequency is excited. An interesting question is forthcoming: how does the state-selective excitation of the $A^2\Pi_{u,1/2}$ state in the photolysis process affect the branching ratios of the two product channels?

Prior to elucidating the underlying mechanism of the observed disparity in the product branching ratios between the ν_1 and ν_3 excitations, it is imperative to delve into the intricacies of the S-loss photodissociation channel of OCS^+ via the $A^2\Pi$ state. Figure 4, adapted from Ref. 34, shows a schematic of the potential energy curves for five low-lying states of OCS^+ (namely, $X^2\Pi$, $A^2\Pi$, $1^4\Sigma^-$, $2^2\Sigma^-$, and $2^2\Delta$, respectively) and the S-loss dissociation reactions along the C–S coordinate. As shown in Fig. 4, the $S^+(^4S_u) + CO(X^1\Sigma^+)$ dissociation channel is adiabatically correlated with the repulsive state of $1^4\Sigma^-$. Hubin-Franskin *et al.*³³ have suggested that the coupling between the $A^2\Pi$ and $1^4\Sigma^-$ states is expected to be relatively weak. Alternatively, they proposed that an internal conversion to the $X^2\Pi$ state, followed by a crossing to the $1^4\Sigma^-$ state, is more likely to occur, ultimately leading to the lowest dissociation limit $S^+(^4S_u) + CO(X^1\Sigma^+)$. Additionally, in 2006, Hirst³⁴ have calculated the low-lying states of OCS^+ by using the multi-reference configuration interaction (MRCI) method. Their findings suggested that the coupling between the $X^2\Pi$ state and the repulsive $1^4\Sigma^-$ state is more probable. Their calculated results indicated that the $X^2\Pi$ state intersects with the $1^4\Sigma^-$ surfaces at an R_{C-S} distance of ~ 2.3 Å.

The second dissociation channel of $S^+(^2D_u) + CO(X^1\Sigma^+)$ is adiabatically correlated with the $X^2\Pi$, $2^2\Sigma^-$, and $2^2\Delta$ states. Two potential pathways have been proposed for this dissociation channel.^{15,31,33,34,45} The first pathway involves internal conversion from the $A^2\Pi$ state to the high vibrational levels of the $X^2\Pi$ state, followed by adiabatic unimolecular decomposition. The other pathway entails direct spin-orbit coupling between the $A^2\Pi$ and the repulsive $2^2\Sigma^-/2^2\Delta$ states. Hirst³⁴ have pointed out that the significance of spin-orbit coupling between the $A^2\Pi$ and $2^2\Sigma^-/2^2\Delta$ states was

minor because the dominant configuration for the $A^2\Pi$ state within the potential well exhibits quite a large deviation from the dissociative states. Chen *et al.*³¹ have calculated the relative energy values for the minimum points along the $A^2\Pi-2^2\Sigma^-$ and $A^2\Pi-2^2\Delta$ intersection seams as 5.21 and 5.35 eV, respectively. The energies of both the intersection points fall outside the experimental photon energy range in this study. It is important to note that in their analysis, the OCS^+ ion maintained a linear configuration with $C_{\infty v}$ symmetry, which may lead to overestimated energy values. Therefore, it is hard to rule out the pathway involving the coupling between $A^2\Pi$ and $2^2\Sigma^-/2^2\Delta$. Furthermore, it was observed that the intersection points of $A^2\Pi-2^2\Sigma^-$ and $A^2\Pi-2^2\Delta$ states were at an R_{C-S} distance of about 1.876 and 1.893 Å, respectively.³¹ Notably, both of these values exceed the R_{C-S} distance (~ 1.795 Å) of the crossing point between the $A^2\Pi$ and $1^4\Sigma^-$ states.

As shown in Fig. 3, for both A ($\nu_1 0 1$) and A ($1 0 \nu_3$) predissociation states, it can be observed that the branching ratio of the electronically excited S^+ channel $S^+(^2D_u) + CO(X^1\Sigma^+)$ exhibits an upward trend as the vibrational energy increases. The observed behavior can be understood by considering the progressive dominance of the $S^+(^2D_u) + CO(X^1\Sigma^+)$ channel as additional rovibrational levels become accessible in accordance to an increase in the total available energy. Nevertheless, as previously illustrated, while possessing a lower overall vibrational energy, the ν_1 excitation is more favorable compared to the ν_3 excitation in the context of generating the higher energy channel $S^+(^2D_u) + CO(X^1\Sigma^+)$. Here, we propose a potential mechanism to explain the observed mode-dependent behavior in the photodissociation dynamics. First, as the vibrational energy increases, there is an enhanced interaction between the $A^2\Pi$ and higher electronically excited states, namely, $1^4\Sigma^-$, $2^2\Sigma^-$, and $2^2\Delta$. This heightened coupling has the potential to lead to an increase in the proportion of the $A^2\Pi \rightarrow 2^2\Sigma^-/2^2\Delta/1^4\Sigma^- \rightarrow$ fragments pathway. The excitation of the ν_1 mode is found to be more favorable for inducing the stretching vibration of the C–S

bond,⁴⁶ hence promoting the elongation of the C–S bond. Furthermore, the R_{C-S} distances for the intersection points of $A^2\Pi-^2\Sigma^-/-^2\Delta$ have substantially greater values, specifically, 1.876 and 1.893 Å, in comparison to the $A^2\Pi-1^4\Sigma^-$ intersection point of around 1.795 Å. Consequently, the excitation of the ν_1 mode is more effective in promoting the coupling between $A^2\Pi$ and $^2\Sigma^-/-^2\Delta$, thereby leading to the generation of $S^+(^2D_u) + CO(X^1\Sigma^+)$.

CONCLUSION

In summary, the photodissociation dynamics of OCS^+ via the $A^2\Pi_{1/2}(\nu_1 0 \nu_3)$ excited states were studied using velocity map ion imaging techniques within the wavelength range of 263–294 nm. High-resolution ion images were recorded for two dissociation channels (I) $S^+(^4S_u) + CO(X^1\Sigma^+)$ and (II) $S^+(^2D_u) + CO(X^1\Sigma^+)$. Significant effects of excited vibrational modes in intermediate states on the relative population of two photodissociation channels were discovered. The experimental findings indicate a notable deviation for the formation of the electronically excited S^+ channel $S^+(^2D_u) + CO(X^1\Sigma^+)$ when the vibrational modes ν_1 and ν_3 were selectively excited. The state-specific effect arising from the excitation of ν_1 was found to promote a greater degree of coupling between $A^2\Pi$ and repulsive states $^2\Sigma^-/-^2\Delta$, compared to the excitation of ν_3 . This study yields valuable insights into the mode and the state-dependent behavior of the dissociation dynamics of ions through multiple vibrationally excited states.

ACKNOWLEDGMENTS

This work was supported by the National Natural Science Foundation of China (Grant Nos. 22125302 and 22327801) and the Innovation Program for Quantum Science and Technology (Grant No. 2021ZD030304).

AUTHOR DECLARATIONS

Conflict of Interest

The authors have no conflicts to disclose.

Author Contributions

Yaling Wang: Data curation (lead); Investigation (lead); Methodology (lead); Validation (lead); Writing – original draft (lead); Writing – review & editing (equal). **Yunfan Zhao:** Data curation (equal); Investigation (equal); Methodology (equal); Software (equal); Validation (lead). **Ning Zhang:** Investigation (equal); Methodology (equal); Software (equal). **Wenxin Wang:** Investigation (equal); Methodology (equal); Software (equal). **Liru Hu:** Investigation (equal); Methodology (equal); Software (equal). **Chang Luo:** Supervision (equal); Writing – review & editing (equal). **Daofu Yuan:** Supervision (equal); Writing – review & editing (lead). **Xiaoguo Zhou:** Supervision (equal); Writing – review & editing (equal). **David H. Parker:** Supervision (equal); Writing – review & editing (equal). **Xueming Yang:** Conceptualization (equal); Supervision (equal). **Xingan Wang:** Conceptualization (lead); Funding acquisition (lead); Project administration (lead); Resources (lead); Supervision (equal); Writing – review & editing (lead).

DATA AVAILABILITY

The data that support the findings of this study are available from the corresponding authors upon reasonable request.

REFERENCES

- 1 F. F. Crim, *Annu. Rev. Phys. Chem.* **44**, 397 (1993).
- 2 R. L. Vander Wal and F. F. Crim, *J. Phys. Chem.* **93**, 5331 (1989).
- 3 R. N. Zare, *Science* **279**, 1875 (1998).
- 4 J. J. Lin *et al.*, *Science* **300**, 966 (2003).
- 5 F. F. Crim, *J. Phys. Chem. A* **100**, 12725 (1996).
- 6 T. Witte *et al.*, *Angew. Chem., Int. Ed.* **40**, 2512 (2001).
- 7 A. Sinha, R. L. Vander Wal, and F. F. Crim, *J. Chem. Phys.* **91**, 2929 (1989).
- 8 T. M. Ticich *et al.*, *J. Chem. Phys.* **87**, 5820 (1987).
- 9 M. Brouard *et al.*, *Chem. Phys. Lett.* **150**, 6 (1988).
- 10 R. L. Vander Wal, J. L. Scott, and F. F. Crim, *J. Chem. Phys.* **94**, 1859 (1991).
- 11 M. D. Lika, J. E. Baggott, and F. F. Crim, *J. Chem. Phys.* **90**, 6266 (1989).
- 12 M. Chin and D. D. Davis, *J. Geophys. Res.: Atmos.* **100**, 8993, <https://doi.org/10.1029/95jd00275> (1995).
- 13 S. A. Montzka *et al.*, *J. Geophys. Res.: Atmos.* **112**, D09302, <https://doi.org/10.1029/2006JD007665> (2007).
- 14 L.-S. Wang *et al.*, *J. Electron Spectrosc. Relat. Phenom.* **47**, 167 (1988).
- 15 J. H. D. Eland, *Int. J. Mass Spectrom. Ion Phys.* **12**, 389 (1973).
- 16 C. Chang, C.-Y. Luo, and K. Liu, *J. Phys. Chem. A* **109**, 1022 (2005).
- 17 M. Somavilla and F. Merkt, *J. Phys. Chem. A* **108**, 9970 (2004).
- 18 R. Kakoschke, U. Boesl, J. Hermann, and E. W. Schlag, *Chem. Phys. Lett.* **119**, 467 (1985).
- 19 R. Weinkauff and U. Boesl, *J. Chem. Phys.* **101**, 8482 (1994).
- 20 W. W. Chen *et al.*, *J. Chem. Phys.* **116**, 5612 (2002).
- 21 J. Huang *et al.*, *J. Chem. Phys.* **115**, 6012 (2001).
- 22 M. Beckert, S. J. Greaves, and M. N. R. Ashfold, *Phys. Chem. Chem. Phys.* **5**, 308 (2003).
- 23 N. Hansen *et al.*, *J. Chem. Phys.* **118**, 10485 (2003).
- 24 O. P. J. Vieuxmaire *et al.*, *Mol. Phys.* **103**, 2437 (2005).
- 25 W. Li *et al.*, *Phys. Chem. Chem. Phys.* **8**, 2950 (2006).
- 26 B. Uselman *et al.*, *J. Phys. Chem. A* **110**, 1278 (2006).
- 27 A. D. Webb *et al.*, *J. Chem. Phys.* **125**, 204312 (2006).
- 28 A. D. Webb, R. N. Dixon, and M. N. R. Ashfold, *J. Chem. Phys.* **127**, 224307 (2007).
- 29 J. Li *et al.*, *J. Chem. Phys.* **134**, 114309 (2011).
- 30 C. Zhang *et al.*, *Phys. Chem. Chem. Phys.* **14**, 2468 (2012).
- 31 B. Z. Chen, H. B. Chang, and M. B. Huang, *J. Chem. Phys.* **125**, 054310 (2006).
- 32 C. Y. R. Wu, T. S. Yihand D. L. Judge, *Int. J. Mass Spectrom. Ion Processes* **63**, 303 (1986).
- 33 M. J. Hubin-Franskin *et al.*, *Chem. Phys.* **209**, 143 (1996).
- 34 D. M. Hirst, *Mol. Phys.* **104**, 55 (2006).
- 35 D. L. Judge and M. Ogawa, *J. Chem. Phys.* **51**, 2035 (1969).
- 36 J. J. Lin, J. G. Zhou, W. C. Shiu, and K. P. Liu, *Rev. Sci. Instrum.* **74**, 2495 (2003).
- 37 S. Yu *et al.*, *J. Phys. Chem. A* **119**, 8090 (2015).
- 38 D. Yuan *et al.*, *J. Phys. Chem. A* **120**, 4966 (2016).
- 39 D. Yuan *et al.*, *J. Phys. Chem. A* **122**, 2663 (2018).
- 40 W. Chen *et al.*, *J. Phys. Chem. Lett.* **10**, 4783 (2019).
- 41 C. Luo *et al.*, *J. Chem. Phys.* **158**, 164304 (2023).
- 42 F. Xu *et al.*, *Chin. J. Chem. Phys.* **33**, 691 (2020).
- 43 T. Xie *et al.*, *J. Phys. Chem. A* **124**, 6420 (2020).
- 44 Z. W. Li *et al.*, *J. Phys. Chem. Lett.* **13**, 815 (2022).
- 45 S. Morse *et al.*, *Int. J. Mass Spectrom.* **184**, 67 (1999).
- 46 S. Stimson, M. Evans, C. Y. Ng, and P. Rosmus, *J. Chem. Phys.* **108**, 6205 (1998).